Contents lists available at ScienceDirect

## Materials & Design

journal homepage: www.elsevier.com/locate/matdes





# Design of La-based MG-Ta composite with high and tailorable properties for solid Ta electrolytic capacitor

Dongjin Chen<sup>a</sup>, Jianan Fu<sup>a</sup>, Shike Huang<sup>a</sup>, Jinbiao Huang<sup>a</sup>, Jian Yang<sup>a</sup>, Shuai Ren<sup>a,b</sup>, Jiang Ma<sup>a,b,\*</sup>

- a Guangdong Key Laboratory of Electromagnetic Control and Intelligent Robots, Shenzhen University, Shenzhen 518060, China
- <sup>b</sup> Shenzhen Key Laboratory of High Performance Nontraditional Manufacturing, College of Mechatronics and Control Engineering, Shenzhen University, Shenzhen 518060. China

#### ARTICLE INFO

Keywords:
Metallic glass
Ta powder
Thermoplastic
Composite
Specific capacitance
Capacitor

#### ABSTRACT

Developing a convenient and efficient way of tantalum (Ta) electrolytic capacitor manufacture process is of great importance in many fields, in which a time-saving and energy-efficient tonology of Ta powder consolidation is also desirable. As a typical way to consolidate Ta powder, powder sintering solves the consolidation difficulty of refractory metal like Ta, while the temperature that required are still high which means high energy costs. In the precent work, we tried to apply metallic glass (MG) as a glue to bond the Ta powder at a low temperature (513 k) and successfully obtained the MG-Ta composite due to the excellent thermoplasty of MG. The bonding mechanism between MG and Ta powder was then investigated and the results showed that the MG and Ta were well combined with each other. Moreover, the MG-Ta composite exhibits high performance enhancement with 57 % increased of specific capacitance and 32 % increased of mechanical property than pure Ta. In addition, the specific capacitance of the composite can be improved via acid etching and the mechanism was investigated. Our results provide a facile approach to consolidate the Ta powder with low cost as well as greatly enhance the performance for its application for solid Ta electrolytic capacitor.

## 1. Introduction

Among many metals with high melting point, Ta has many good properties, including excellent plasticity [1,2] and biocompatibility [3,4]; the Ta oxide generated on the surface of Ta metal is extremely resistant to corrosion [5,6] and is also an excellent dielectric material [7,8]. As a result, Ta has a wide range of applications in the fields of medicine, chemistry and electronic engineering. Especially in the electronics industry, solid Ta electrolytic capacitors made of Ta powder are widely used due to its high specific capacitance [9,10]. In addition, because of its good biocompatibility, Ta has a wide range of prospects in dentistry applications and artificial bone joints fabrication [11–13].

Porous Ta is one of the typical applications for Ta metal, and powder metallurgical method is one of the common preparation methods using Ta powder due to the high melting point of Ta [14]. Moreover, Ta anode in the solid Ta electrolytic capacitor is one of the widely uses of porous Ta made by Ta powder. The classical Ta anode fabrication process would first focus on the preparation of Ta powder, where the conventional way

is to reduce  $K_2TaF_7$  using MR in molten salt [15]; whereas the novel approach is to directly carry out the reduction of  $Ta_2O_5$  to prepare finer Ta powder [10]. The prepared tantalum powder is then usually subjected to procedures such as ball milling, high temperature heat treatment, deoxidization, etc.; finally, by means of powder metallurgy, the Ta powder is sintered at a temperature of around 1475 K into bulk pellets of the desired shape for subsequent steps such as the formation of the oxide layer. From the above process, we note that very high temperatures are typically required for the sintering of Ta powder, and combined with the time required for heating and cooling, the process is inevitably energy and time consuming. Now the high-cost problem can be solved by using amorphous alloys as the bonding agent to bond the powders as a bulk composite (the metallic glue strategy).

Amorphous alloy materials, also known as MG, which combine the properties of metal and glass, have attracted attention since their discovery for their excellent properties [16–24]. The most special property of amorphous alloy materials is that when the temperature of the material rises above a certain temperature, the alloy will become soft and

<sup>\*</sup> Corresponding author at: Guangdong Key Laboratory of Electromagnetic Control and Intelligent Robots, Shenzhen University, Shenzhen 518060, China. E-mail address: majiang@szu.edu.cn (J. Ma).

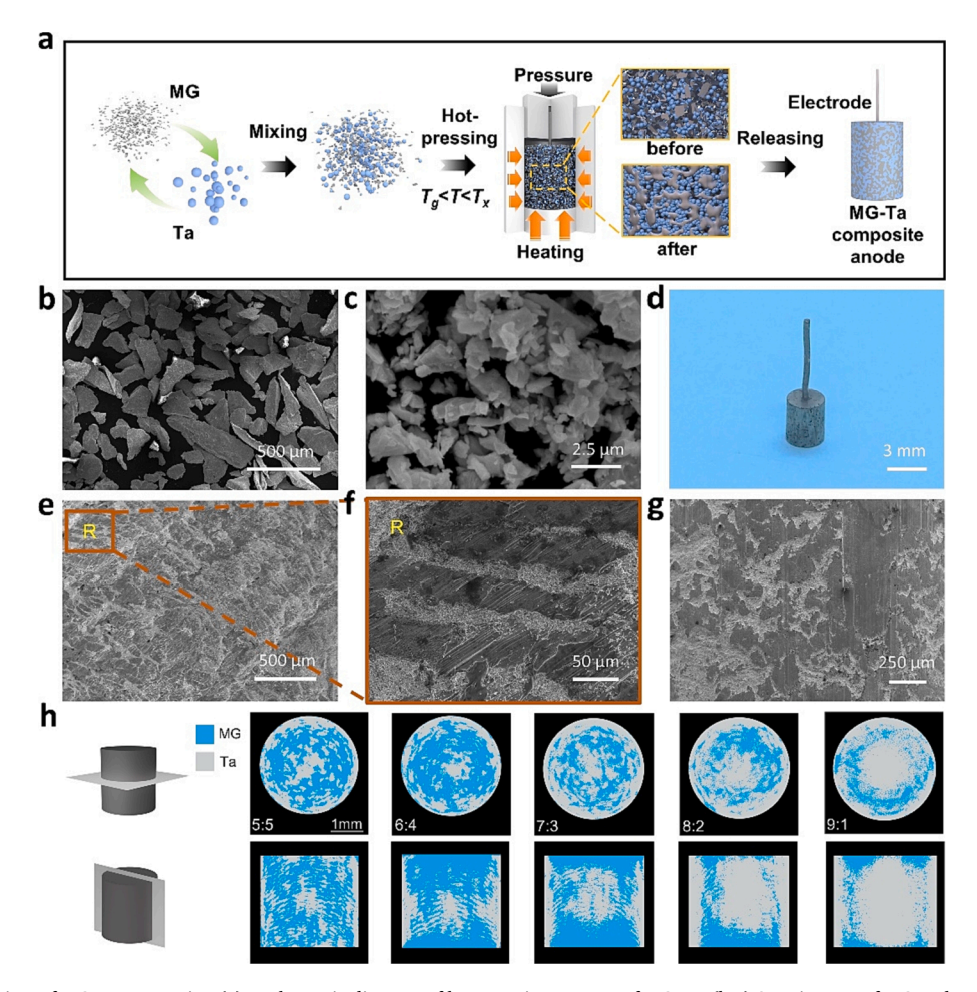


**Fig. 1.** Bonding mechanism of MG-Ta composite. (a) a schematic diagram of hot-pressing process of MG-Ta. (b-c) SEM images of MG and Ta powder respectively. (d) Photography picture of MG-Ta composite anode. (e-f) SEM images of the cross-section of the sample. (g) SEM image of the surface of the composite. (h) The CT images of two sections corresponding to MG-Ta composites with five different mass ratios.

flow viscously under the action of pressure [25–31]. If the temperature keeps rising, its viscosity characteristics will increase sharply until the temperature reaches a certain point [32]. Over that point, the amorphous alloy will change from the amorphous state to the crystalline state [33,34]. Those two temperature points are called glass transition temperature ( $T_g$ ) and crystallization temperature ( $T_x$ ), respectively, and the interval between them called the supercooled liquid region (SLR) [35]. The SLR of metallic glass is much lower than the melting point of the material, which make it possible to gain excellent thermoplastic forming ability at low temperature [25].

The thermoplastic forming ability of amorphous alloy not only can be used for micro and nano processing [36–38], but also has been used as metallic glues to cemented with other materials to form bulk composites with tunable material properties [39]. Such bulk composites provide an alternative forming method to powder metallurgy for the preparation of some refractory metals such as Ta and niobium into bulk metallic materials. Among many kinds of MG, lanthanum-based metal glasses [40,41] has a low  $T_{\rm g}$  (less than 465 K) and a wide SLR (about 50 K) [39], which is less than 1/4 of the temperature used to cement Ta powder using powder metallurgy. Meanwhile, this material has a small coefficient of thermal expansion [42,43], which indicates that the metal glue strategy has a natural advantage in energy saving and emission reduction to meet the demand of green development in the current environment.

In this study, we made an attempt to solidify Ta powder using the metal glue strategy and through our tests, we obtained an increase in specific capacitance of up to 57 % compared to pure Ta powder, as well

as a 32 % increase in the compressive strength of the composite with the addition of only 10 wt% of the metal glue. In order to investigate the changes in the properties of the MG-Ta composites obtained metallic glue strategy and the mechanism behind them, La-based amorphous alloy was chosen as the metal glue because of its low SLR and excellent mechanical properties at room temperature, which can significantly reduce the processing temperature and time. During the study we also found that the electrical properties of the composites will improve after a period of time under the influence of acid corrosion, and the mechanism of this phenomenon was explained and experimentally verified. The results of this study further confirmed the feasibility of amorphous alloy as a metal glue to cement Ta powder, and also found that the amorphous alloy in the MG-Ta composite not only plays a bonding and cementing role, but also has a gaining effect on the electrical and mechanical properties of Ta powder, and by adjusting the content of amorphous alloy can achieve the performance regulation of the composite material. The unique structure of MG in the bulk allows the mechanical properties of the MG-Ta bulk to be significantly improved. This provides a new and viable strategy for forming Ta and other high melting point metals into blocks, and is more energy and time efficient to meet future demands for increased productivity and environmentally friendly technologies.

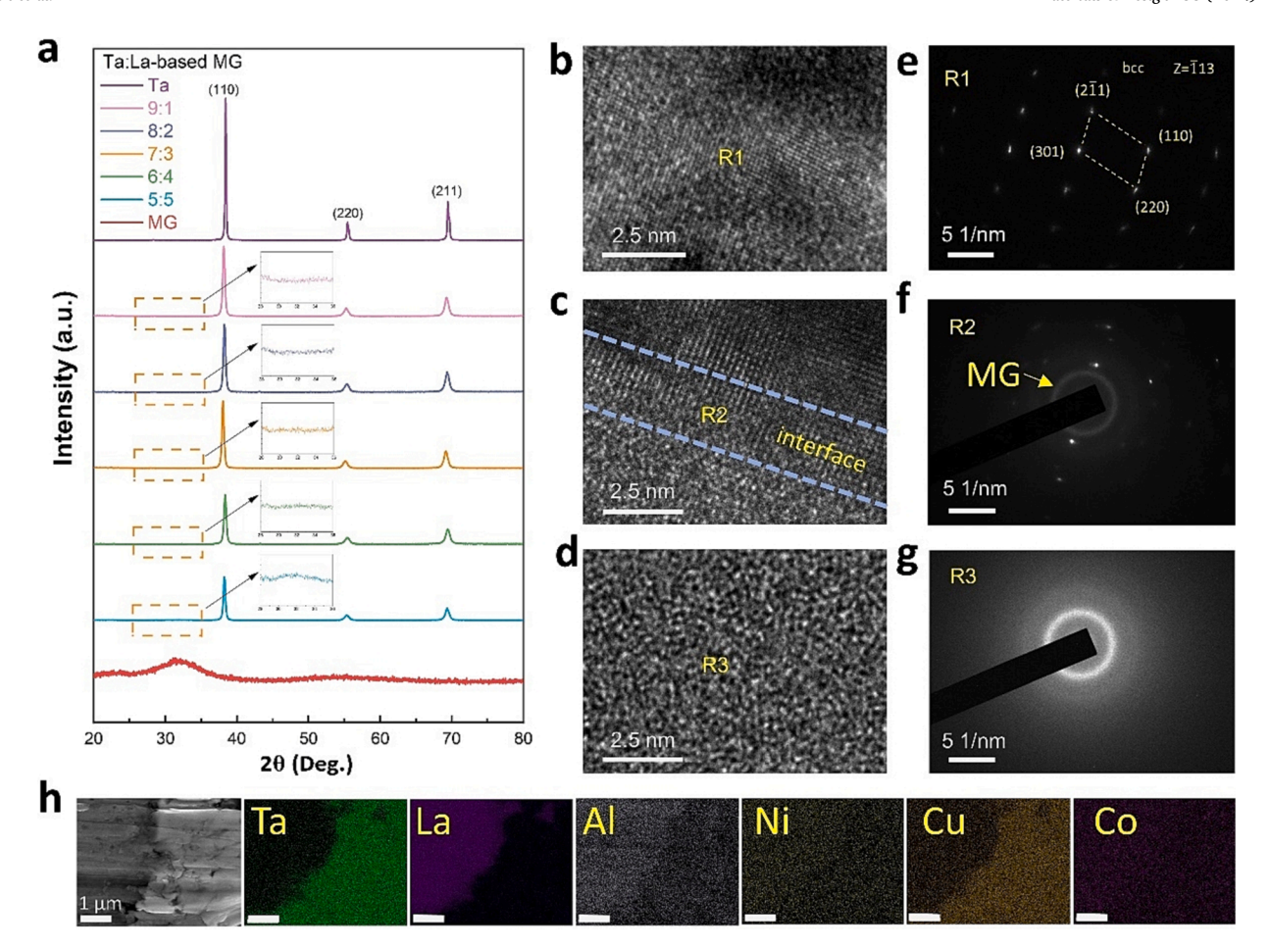


Fig. 2. Atomic characterization of MG-Ta composite. (a) The XRD patterns of different materials. (b-d) The high-resolution TEM images of the Ta region, interface region and MG region respectively. (e-g) The corresponding diffraction patterns of R1, R2 and R3 region from b-d. (h) The elemental distribution of the sample at the interface.

## 2. Experimental methods and materials

## 2.1. Preparation of materials

The La-based MG used in the experiments is  $La_{55}Al_{25}Ni_5Cu_{10}Co_5$ , because it has a low and very wide SLR, while maintaining good thermoforming ability. The MG is fabricated in the lab using Vacuum-Arc-Melting-Furnace and Vacuum-Melt-Spinner, the purity of the composition can be seen in Table S1; Ta powder was purchased from the market and its powder size and composition can be found in Table S2.

## 2.2. Bonding process

A specific proportion of lanthanum-based amorphous alloy powder is first mixed thoroughly with Ta powder (mass ratios of Ta: MG are 5:5, 6:4, 7:3, 8:2, 9:1, respectively) and then placed in a 3 mm diameter mold cavity. The mold is then placed in a hot-pressing machine and heated to approximately 513 K in argon atmosphere (slightly below the  $T_x$  point of the MG, when it is at its softest state), followed by pressurization to 5 kN at a rate of 0.05 mm·s<sup>-1</sup> and held for approximately 60 s. The pressure is then rapidly reduced to 0 kN and the mold is cooled down by water cooling, and the sample is removed from the mold after they are at room temperature.

## 2.3. Multi-scale characterizations of the composite

The La-based MG and Ta powders and their composites obtained by hot pressing was detected by X-ray diffraction (XRD; RIGAKU

miniflex600) with Cu Ka radiation. And differential scanning calorimetry (DSC; PerkinElmer DSC-8000) at a heating rate of 20 K min1 was used to clarify the  $T_g$  and  $T_x$  of the La-based powder (Fig. S1). The micro morphology of all the materials was observed using the scanning electron microscope (SEM; Fei quanta FEG 450) instrument, and its energy disperse spectroscopy (EDS) was used to characterize the elemental distribution of the composites. The atomic structure was characterized using JEM-2100F transmission electron microscopy (TEM). The TEM samples were prepared on a FEI Scios SEM/FIB dual beam system. The CT pictures of the samples were obtained from the skysCan2211/ZEISS Xradia520/NIKON XTH 225/320 machine. When testing the compressive property of the MG-Ta composite, the samples were made into the cylinder shape with a length/diameter ratio of 1.5 according to the ASTM standard, then they were tested by Z050TEWwith a strain rate of 0.001 s<sup>-1</sup>) at room temperature. In order to measure the specific capacitance of the Ta powder in MG-Ta composite, the WB6000 was used to test the capacitance of the composite in sulfur acid (H<sub>2</sub>SO<sub>4</sub>, 38 wt %) solution, the setup can be seen in Fig. S2.

## 3. Results and discussions

## 3.1. Bonding mechanism

Fig. 1a is the schematic diagram of the MG-Ta composite anode's preparation process, through the process, the MG and Ta powder with an electrode were bonded into dense and firm pellets as anodes. As shown in Fig. 1e, f and g, no obvious cracks separating the two phases are observed in either the internal section or the surface, indicating the

Materials & Design 238 (2024) 112743

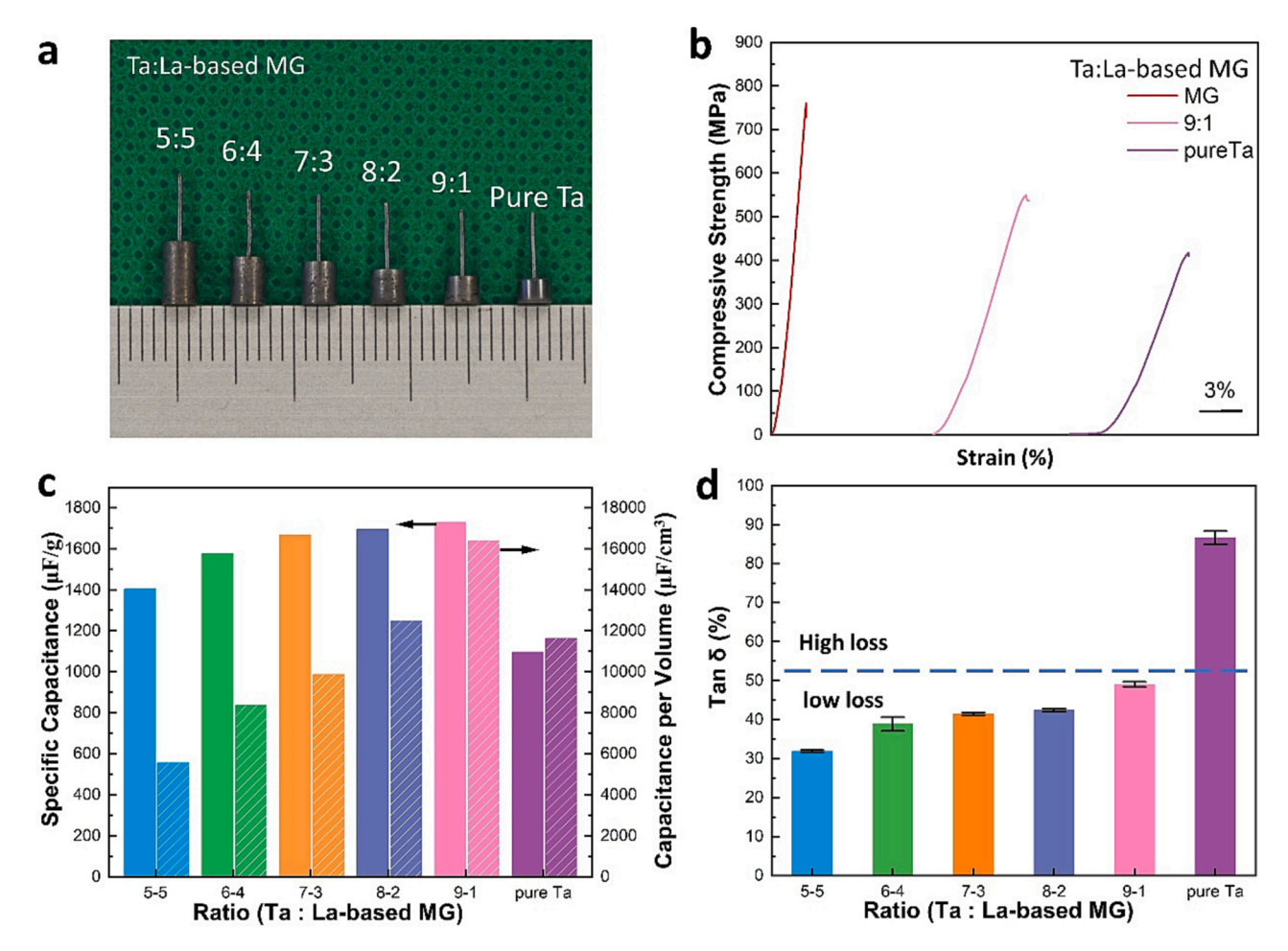


Fig. 3. Properties investigation of MG-Ta composite. (a) The photography pictures of anodes made by MG-Ta composites with different mass ratios. (b) The compressive strength of the MG-Ta bulk composites. (c) The specific capacitance of the composite anodes. (d) The Tan  $\delta$  of the composite anodes.

homogeneity and tightness of MG-Ta composite.

To further investigate the inner structure of the bulk composite, a CT scan was applied to scan the samples with five mass fractions (Ta: MG = 5.5, 6:4, 7:3, 8:2, 9:1, respectively). As shown in Fig. 1h, the cross-sections of the samples are on the top with the corresponding longitudinal sections images on the bottom. The CT images of cross section reveal a roughly interwoven and uniform distribution between the Ta and MG region of the samples with mass fraction of 5:5 to 7:3. In contrast, the MG of 9:1 composite is uniformly distributed in a ring around the axis of the sample, which is also reflected in the longitudinal section image. The distribution situation of the 8:2 sample is between 7:3 and 9:1, and the Ta region in the center of the cross-section and longitudinal section begins to expand when compared to the 7:3 sample, showing a transitional state.

The different distribution in the samples indicates that the ratio of the two materials in the MG-Ta composite will affect the formation state of the internal structure of the bulk composite. Moreover, the stacked structure mentioned in Fig. 1e-f is shown more visually from the CT scans images. Even for the 8:2 and 9:1 samples with different cross-sectional distribution, the amorphous alloys are also stacked in the longitudinal direction. This structure is caused by the fact that the amorphous alloy inside the block basically flows along the transverse direction during the hot-pressing process, and this structure has a significant impact when properties of the MG-Ta composite were explored.

Furthermore, an XRD analysis was applied to examine the crystalline state of the composite. The XRD patterns of composite with different constituent are shown in Fig. 2a, which demonstrates the amorphous peaks of the La-based amorphous alloy and the characteristic peaks of

the Ta powder. As seen from the 5:5 curve, the characteristic peaks of both materials are reflected in the curve, indicating the mixed state of both materials. And from 6:4 onwards, the amorphous peak of MG becomes very inconspicuous, which is due to the very large difference compared to the characteristic peak of the amorphous alloy with the crystal peak of Ta powder. It is also found that the intensity of the Ta powder crystal peaks of the composite gradually increases as the MG content decreases, but the difference is very large compared to the intensity of the pure Ta crystal peaks.

To further investigate the bonding situation of the interface between MG and Ta, the composites were subjected to TEM characterization and energy spectrum analysis. Fig. 2b, d, f shows the high-resolution TEM images of Ta powder, bonding interface and MG in the MG-Ta composite, respectively, from which it can be seen that the three regions show different atomic structures, the Ta powder region is a classical crystal structure, the atoms in the MG region are in a disordered state, and the bonding interface is a mixture of the two structures, reflecting that the bonding of MG and Ta powder is at the atomic level. In addition, three positions (R1, R2, R3) were selected from the HRTEM image for diffraction analysis, and the diffraction results obtained are shown in Fig. 2 c, e, g. The diffraction results at position R1 show a regular lattice structure, which corresponds to the atomic structure of the Ta powder in the TEM and the characteristic peaks of the crystal shown in the XRD pattern; the diffraction results at position R3 show a bright diffraction halo, which corresponds to the amorphous state of the atoms; the diffraction results at position R2 are exactly a combination of the results of R1 and R3, and the diffractogram contains both spots and haloes, which correspond to the mixed state of two atomic arrangements in the

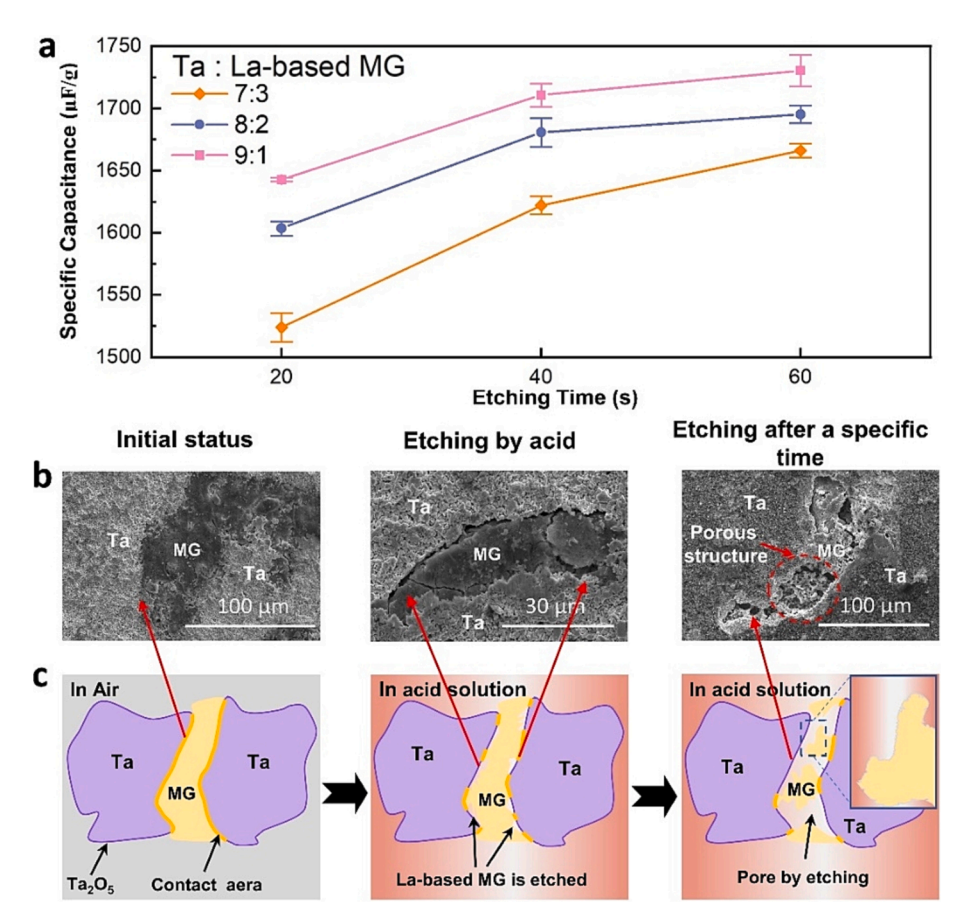


Fig. 4. Electric property enhancement by acid etching. (a) The specific capacitance pattern vs etching time. (b) The SEM images of the sample surface in different etching state. (c) A schematic diagram of the etching process.

interface.

The SEM image of the interface and its corresponding energy spectrum as shown in Fig. 2h also clearly reveals the tight combination of two materials. The elemental distribution can be seen from the energy spectrum and it shows that the elemental diffusion happens in the interface which further indicates that the amorphous alloy and Ta powder reach the atomic level bonding state at the bonding interface, illustrating the tightness of the bonding with the two materials.

## 3.2. Property enhancement

To investigate the property changes of Ta powder after adding Labased amorphous alloy as the bonding agent, the bulk composites with mass fractions of 5:5, 6:4, 7:3, 8:2 and 9:1 were used as anodes, as shown in Fig. 3a. The capacitance values were measured in the capacitance testing device and divided by the mass of Ta contained in the composites (fixed at 0.15 g) to obtain the corresponding specific capacitance values. The same hot-pressing parameters were also used to press the pure Ta powder into anode blocks for capacitance testing to obtain their specific capacitance values.

The experimentally obtained results are shown in Fig. 3c, it can be seen that all the specific capacitance in weight of MG-Ta pellets are higher than pure Ta pellet. The biggest performance gains were made by MG-Ta with 9:1 mass ratio, about 57 % higher than the pure Ta pellet. The capacitance values per volume was also calculated (shown in right of Fig. 3c), the results shows that the specific capacitance of volume decreases as the content of MG increases as the capacitance values per weight do, but the values begin becoming lower than pure Ta from the MG content over 30 % in mass, which indicates the negative effect of volume increasement the La-based MG brings about. However, the value

of "8:2" and "9:1" are still higher the pure Ta, the capacitance per volume enhancement of "9:1" reached 40 % over pure Ta. In addition, the tan  $\delta$  value of Fig. 3d is a parameter to measure the capacitance loss during the capacitance test, and the lower the value, the better the electrical properties of the material.

It is imperative to clarify the mechanism of the MG's effect on MG-Ta composites. The specific capacitance of Ta powder is influenced by several factors, including the porosity of the pellet [10], the thickness of the  $\rm Ta_2O_5$  layer (shown in Fig. S4) on the surface of the Ta powder particles, etc. [7] Although the incorporation of MG does not change the structure of Ta powder particles, as shown in Fig. S5, it will firstly fill in the pores formed by the interstices of Ta powder particles as a bonding agent in the pellet. According to H.S. Ryu [10], the size of these pores determines the surface area of the Ta powder after it solidifies into a pellet, which in turn affects its capacitive performance as an anode. Therefore, these pores will decrease due to the increase of MG content, which leads to the decrease of the actual surface area of the pellet, and ultimately leads to the consequent decrease of the capacitance performance as shown in Fig. 3c.

However, in terms of the volumetric specific capacitance, the MG-Ta pellet with mass ratio of 9:1 still has a significant performance enhancement over the pure Ta pellet. The source of this enhancement is that MG acts as a bonding agent as well as the "necking" between Ta powder particles, as shown in Fig. S5. According to the results of Fig. 2, the bonding state between MG and Ta powder was reached at the atomic level; Furthermore, to carry out a comprehensive analysis to the effect MG, the La-based MG was tested for its dielectric information. As the results shown in Fig. S6, the electrical property of MG is close to that of a conductor, which means that the connecting effect of MG on Ta powder particles is similar to the "necking" of Ta powder during sintering, and

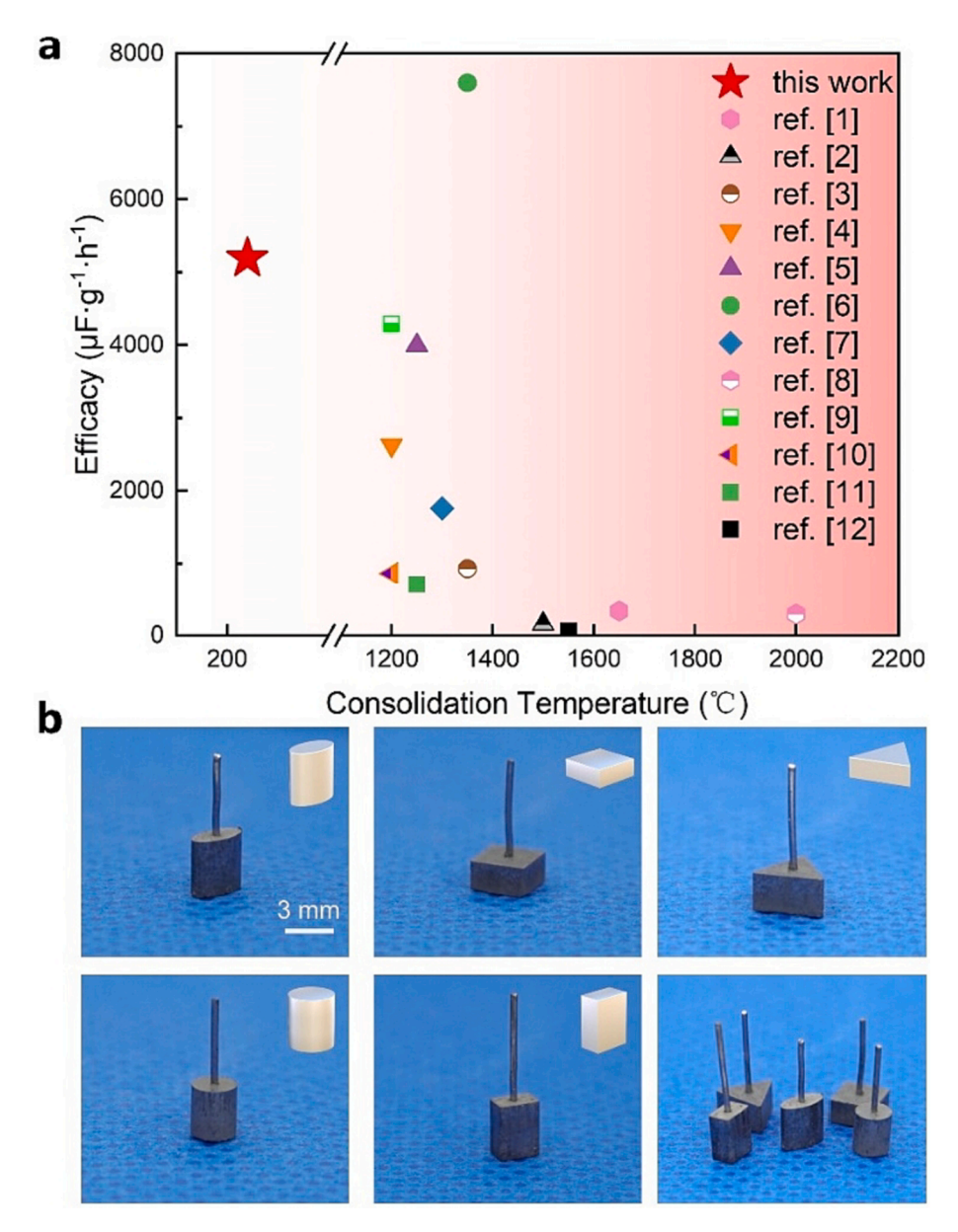


Fig. 5. Efficiency and forming flexibility of MG-Ta composite. (a) Comparison of electric performance per consolidation time and temperature of this work and other references. (b) Different shapes of anodes made by MG-Ta composite for capacitor manufacture.

such a connection serves as a conduction of different Ta powder particles. In other words, the use of MG as a bonding agent can play a role in compensating for the poor bonding between the particles of pure Ta powder under the same low-temperature hot-pressing parameter, so that the MG-Ta pellet can maintain good capacitive performance.

In addition, the mechanical properties of the composites were also tested, and as shown in Fig. 3b, the La amorphous alloy exhibited a high compressive strength (760 MPa), 83% higher than that of the Ta powder block (416 MPa), while the compressive strength of the composite with 10% content of MG addition was 32% higher than that of the pure Ta powder block. The longitudinal cross-sectional view according to the CT diagram in Fig. 1h demonstrates that the amorphous alloy is showing a tile-like stacked structure in the direction of compression of the composite block, and this structure has a significant contribution to the compressive strength, achieving a significant strength enhancement effect of the composite. The data in Fig. 3 shows that La-based amorphous alloy is not only used as a metallic glue in the composite material for bonding and enhancing the mechanical properties, but also has a very good effect on the electrical properties of Ta powder.

Meanwhile, an interesting phenomenon was observed during the testing of capacitance. As shown in Fig. 4a, it was found that the specific capacitance of the MG-Ta composite showed an increasing trend when the composite stayed in the testing acid solution for a specific time. Noting that La-based amorphous alloys are susceptible to acid corrosion, when the composite sample is immersed in the test solution for an extended period of time, the joint state between the Ta powder region and the amorphous alloy region of the sample changes due to corrosion, which changes the "necking" between the adjacent Ta powder regions, as described earlier.

To further investigate the mechanism of this phenomenon, the surface of the composites of different etching states were observed using SEM, as shown in Fig. 4b. It can be seen that before the corrosion, there is a good bonding interface between the amorphous alloy and the Ta powder, and the adjacent Ta powder regions remain in a fixed necking state. When in acidic solution, due to the strong corrosion resistance of  $Ta_2O_5$  oxide layer on the surface of Ta powder, the Ta powder region will not change, while the La-based amorphous alloy sandwiched in the middle starts to be corroded and pores appear. After a period of

corrosion, the pores gradually expand to form holes up to the Ta powder area connecting the two sides and the porous structure was formed by acid etching.

Fig. 4c schematically depicts the changing process of how the Labased MG was etching by the acid. As mentioned earlier, the addition of amorphous alloy makes an impact on the specific capacitance value, and the experimental results show that the loss of amorphous alloy also brings an impact on the electrical properties and improves the specific capacitance of the sample. According to the changes revealed in Fig. 4b and c, the amorphous alloy leaves a porous-like structure on the surface of the sample after it has been etched, and the Ta powder covered by the amorphous alloy is exposed on the surface of the sample. The change brought about by this structure is an increase in the surface area of this composite block, therefore corresponds to an increase in the specific surface area of the Ta powder, which explains the increase in the specific capacitance value in the experimental results.

The results show that for bulk composite made by adding amorphous as a binder with Ta powder, not only can the electrical properties of the Ta powder be regulated by adjusting the content of the amorphous alloy, but for composites with same weight fraction, the electrical properties of the composite can be further increased by means of proper etching of the amorphous alloy. Similar to the method of using the solubility of solids to create porous structures [44], this study uses the susceptibility of the material to corrode to produce corresponding structural changes and thus alter the material's properties.

Moreover, Fig. 5a summarizes the comparation of the process parameter (specific capacitance, time and consolidation Temperature) between this work and other methods that mentioned from some references (see in supplementary information). Here we divided the specific capacitance by the time of the consolidation to show the efficiency of the process from different methods. The data in Fig. 5a shows that the MG-Ta has lowest consolidation temperature among all the other works, which indicates a significant advantage of lowering down the energy cost. Meanwhile, the time required for the pellet's preparation is quite low, leading to a secondly high capacitance performance that can be obtained per hours. It can be seen that the low cost both in time and energy while keeping a good performance of electric property demonstrates the advantages and broad application prospects of using MG as a metal bonding agent. In addition, Fig. 5b also shows the process flexibility of making different shapes of anodes for capacitor manufacture. That further means that the forming strategy of MG-Ta composite meets both the needs of efficiency and energy saving simultaneously and have a larger potential application scenario.

#### 4. Conclusion

In summary, the MG-Ta composite was fabricated by the metallic glue strategy in this work, which is a convenient and a property-controllable way. Additionally, we investigate the bonding mechanism and properties of the MG-Ta composites. The experimental results shows that the MG and Ta powder are well bonded due to the good flowability of La-based MG. Moreover, compared to the pure Ta, the electric performance and compressive strength of the composite was reached a 57 % and 32 % increase, respectively. Furthermore, the specific capacitance of the MG-Ta can be regulated by acid etching. Our research result provided a new strategy to consolidate the Ta powders, which has a low cost and forming flexibility to make it possible for MG-Ta composite to be applied in electric devices fields and other potential areas.

## CRediT authorship contribution statement

**Dongjin Chen:** Data curation, Formal analysis, Investigation, Validation, Writing – original draft. **Jianan Fu:** Methodology, Writing – review & editing. **Shike Huang:** Methodology. **Jinbiao Huang:** Methodology. **Jian Yang:** Resources, Supervision, Writing – review & editing. **Shuai Ren:** Supervision. **Jiang Ma:** Resources, Supervision, Writing –

review & editing.

#### Declaration of competing interest

The authors declare that they have no known competing financial interests or personal relationships that could have appeared to influence the work reported in this paper.

## Data availability

The data that support the findings of this study are available from the corresponding author upon reasonable request.

## Acknowledgements

The work was supported by the National Key Research and Development Program of China (Grant No. 2018YFA0703605), the Key Basic and Applied Research Program of Guangdong Province, China (Grant Nr. 2019B030302010), the NSF of China (Grant Nr. 51871157). The authors are grateful for the assistance on the microscope observation received from the Electron Microscope Center of Shenzhen University.

## Appendix A. Supplementary data

Supplementary data to this article can be found online at https://doi.org/10.1016/j.matdes.2024.112743.

#### References

- [1] R.W. Buckman, New applications for tantalum and tantalum alloys, JOM 52 (3) (2000) 40–41 https://doi.org/10.1007/s11837-000-0100-6
- [2] S.M. Cardonne, P. Kumar, C.A. Michaluk, H.D. Schwartz, Tantalum and its alloys, Int. J. Refract. Met. Hard Mater. 13 (4) (1995) 187, https://doi.org/10.1016/0263-4368(95)94023-r
- [3] J. Black, Biological performance of tantalum, Clin. Mater. 16 (3) (1994) 167–173, https://doi.org/10.1016/0267-6605(94)90113-9.
- [4] V.K. Balla, S. Bose, N.M. Davies, A. Bandyopadhyay, Tantalum-a bioactive metal for implants, JOM 62 (7) (2010) 61–64, https://doi.org/10.1007/s11837-010-0110-
- [5] X. Wang, B. Y. Ning, X. B. Pei, Tantalum and its derivatives in orthopedic and dental implants: Osteogenesis and antibacterial properties, Colloids Surf., B 208 (2021) 16. https://doi.org/10.1016/j.colsurfb.2021.112055.
- [6] F. Carraro, A. Bagno, Tantalum as trabecular metal for endosseous implantable applications, Biomimetics 8 (1) (2023) 21, https://doi.org/10.3390/ biomimetics8010049
- [7] D.L. Pulfrey, P.S. Wilcox, L. Young, Dielectric properties of Ta2O5 thin films,
   J. Appl. Phys. 40 (10) (1969) 3891, https://doi.org/10.1063/1.1657112.
- [8] K.M.A. Salam, H. Fukuda, S. Nomura, Effects of additive elements on improvement of the dielectric properties of Ta2O5 films formed by metalorganic decomposition, J. Appl. Phys. 93 (2) (2003) 1169–1175, https://doi.org/10.1063/1.1532940.
- [9] J.S. Yoon, B.I. Kim, Characteristics and production of tantalum powders for solidelectrolyte capacitors, J. Power Sources 164 (2) (2007) 959–963, https://doi.org/ 10.1016/j.jpowsour.2006.11.035.
- [10] H.S. Ryu, H. Nersisyan, K.T. Park, J.H. Lee, Porous tantalum network structures exhibiting high electrochemical performance as capacitors, Journal of Energy Storage 34 (2021) 10, https://doi.org/10.1016/j.est.2020.102222.
- [11] P. Alberius, Bone reactions to tantalum markers a scanning electron-microscopic study, Acta Anat. 115 (4) (1983) 310–318, https://doi.org/10.1159/000145707.
- [12] J.D. Bobyn, R.A. Poggie, J.J. Krygier, D.G. Lewallen, A.D. Hanssen, R.J. Lewis, A.S. Unger, T.J. O'keefe, M.J. Christie, S. Nasser, J.E. Wood, S.D. Stulberg, M. Tanzer, Clinical validation of a structural porous tantalum biomaterial for adult reconstruction, J BONE JOINT SURG AM 86A(2004) 123-129. https://doi.org/10.2106/00004623-200412002-00017.
- [13] Y.D. Liu, C.Y. Bao, D. Wismeijer, G. Wu, The physicochemical/biological properties of porous tantalum and the potential surface modification techniques to improve its clinical application in dental implantology, Mater. Sci. Eng., C 49 (2015) 323–329, https://doi.org/10.1016/j.msec.2015.01.007.
- [14] J.H. Qin, Q. Chen, C.Y. Yang, Y. Huang, Research process on property and application of metal porous materials, J. Alloys Compd. 654 (2016) 39–44, https:// doi.org/10.1016/j.jallcom.2015.09.148.
- [15] H.I. Won, H.H. Nersisyan, C.W. Won, Combustion synthesis-derived tantalum powder for solid-electrolyte capacitors, J. Alloys Compd. 478 (1–2) (2009) 716–720, https://doi.org/10.1016/j.jallcom.2008.11.140.
- [16] A. Inoue, B.L. Shen, H. Koshiba, H. Kato, A.R. Yavari, Cobalt-based bulk glassy alloy with ultrahigh strength and soft magnetic properties, Nat. Mater. 2 (10) (2003) 661–663, https://doi.org/10.1038/nmat982.

- [17] W.H. Wang, C. Dong, C.H. Shek, Bulk metallic glasses, Mater. Sci. Eng. R-Rep. 44 (2–3) (2004) 45–89, https://doi.org/10.1016/j.mser.2004.03.001.
- [18] M.F. Ashby, A.L. Greer, Metallic glasses as structural materials, Scripta Mater. 54 (3) (2006) 321–326, https://doi.org/10.1016/j.scriptamat.2005.09.051.
- [19] W. Klement, R.H. Willens, P. Duwez, Non-crystalline structure in solidified gold-silicon alloys, Nature 187 (4740) (1960) 869–870, https://doi.org/10.1038/187869b0.
- [20] R. Vaidyanathan, M. Dao, G. Ravichandran, S. Suresh, Study of mechanical deformation in bulk metallic glass through instrumented indentation, Acta Mater. 49 (18) (2001) 3781–3789, https://doi.org/10.1016/s1359-6454(01)00263-4.
- [21] H. Guo, P.F. Yan, Y.B. Wang, J. Tan, Z.F. Zhang, M.L. Sui, E. Ma, Tensile ductility and necking of metallic glass, Nat. Mater. 6 (10) (2007) 735–739, https://doi.org/ 10.1038/nmat/1984
- [22] J. Hafner, Theory of the formation of metallic glasses, PhRvB 21 (2) (1980) 406–426, https://doi.org/10.1103/PhysRevB.21.406.
- [23] J. Schroers, W.L. Johnson, Highly processable bulk metallic glass-forming alloys in the Pt-Co-Ni-Cu-P system, Appl. Phys. Lett. 84 (18) (2004) 3666–3668, https://doi.org/10.1063/1.1738945.
- [24] N. Li, Y. Chen, M. Jiang, D. Li, J. He, Y. Wu, L. Liu, A thermoplastic forming map of a Zr-based bulk metallic glass, Acta Mater. 61 (6) (2013) 1921–1931, https://doi. org/10.1016/j.actamat.2012.12.013
- [25] W.H. Wang, Bulk metallic glasses with functional physical properties, Adv. Mater. 21 (45) (2009) 4524–4544, https://doi.org/10.1002/adma.200901053.
- [26] Z. Li, Z. Huang, F. Sun, X. Li, J. Ma, Forming of metallic glasses: mechanisms and processes, Mater. Today Adv. 7 (2020), https://doi.org/10.1016/j. mtadv.2020.100077.
- [27] J. Ma, X.Y. Zhang, D.P. Wang, D.Q. Zhao, D.W. Ding, K. Liu, W.H. Wang, Superhydrophobic metallic glass surface with superior mechanical stability and corrosion resistance, Appl. Phys. Lett. 104 (17) (2014), https://doi.org/10.1063/ 1.4874275.
- [28] H.Z. Li, Z. Li, J. Yang, H.B. Ke, B.A. Sun, C.C. Yuan, J. Ma, J. Shen, W.H. Wang, Interface design enabled manufacture of giant metallic glasses, Sci. China Mater. 64 (4) (2021) 964–972, https://doi.org/10.1007/s40843-020-1561-x.
- [29] G. Duan, A. Wiest, M.L. Lind, J. Li, W.K. Rhim, W.L. Johnson, Bulk metallic glass with benchmark thermoplastic processability, Adv. Mater. 19 (23) (2007) 4272–4275, https://doi.org/10.1002/adma.200700969.
- [30] J. Ma, X. Liang, X. Wu, Z. Liu, F. Gong, Sub-second thermoplastic forming of bulk metallic glasses by ultrasonic beating, Sci. Rep. 5 (1) (2015) 17844, https://doi. org/10.1038/srep17844.

- [31] F. Sun, B. Wang, F. Luo, Y.Q. Yan, H.B. Ke, J. Ma, J. Shen, W.H. Wang, Shear punching of bulk metallic glasses under low stress, Mater. Des. 190 (2020) 108595, https://doi.org/10.1016/j.matdes.2020.108595.
- [32] B.A. Legg, J. Schroers, R. Busch, Thermodynamics, kinetics, and crystallization of Pt57.3Cu14.6Ni5.3P22.8 bulk metallic glass, Acta Mater. 55 (3) (2007) 1109–1116, https://doi.org/10.1016/j.actamat.2006.09.024.
- [33] J.H. Gibbs, E.A. Dimarzio, Nature of the glass transition and the glassy state, J. Chem. Phys. 28 (3) (1958) 373–383, https://doi.org/10.1063/1.1744141.
- [34] J. Schroers, Processing of bulk metallic glass, Adv. Mater. 22 (14) (2010) 1566–1597, https://doi.org/10.1002/adma.200902776.
- [35] M.W. Chen, A brief overview of bulk metallic glasses, NPG Asia Mater. 3 (2011) 82–90, https://doi.org/10.1038/asiamat.2011.30.
- [36] Y. Saotome, K. Imai, S. Shioda, S. Shimizu, T. Zhang, A. Inoue, The micronanoformability of Pt-based metallic glass and the nanoforming of threedimensional structures, Intermetallics 10 (11–12) (2002) 1241–1247, https://doi. org/10.1016/s0966-9795(02)00135-8.
- [37] J.N. Fu, Z.Y. Huang, J. Yang, J. Ma, J. Shen, Nano-forming of the rare earth La-based metallic glass, J. Non-Cryst. Solids 558 (2021) 7, https://doi.org/10.1016/j.inoncrysol.2021.120682.
- [38] R.C. Sekol, M. Carmo, G. Kumar, F. Gittleson, G. Doubek, K. Sun, J. Schroers, A. D. Taylor, Pd-Ni-Cu-P metallic glass nanowires for methanol and ethanol oxidation in alkaline media, Int. J. Hydrogen Energy 38 (26) (2013) 11248–11255, https://doi.org/10.1016/j.ijhydene.2013.06.017.
- [39] J.A. Fu, J. Yang, K. Wu, H.J. Lin, W.N. Wen, W.Q. Ruan, S. Ren, Z.X. Zhang, X. Liang, J. Ma, Metallic glue for designing composite materials with tailorable properties, Mater. Horiz. 8 (6) (2021) 1690–1699, https://doi.org/10.1039/ dlmb0521a
- [40] A. Inoue, K. Kita, T. Zhang, T. Masumoto, An Amorphous La55Al25Ni20 Alloy Prepared by Water Quenching, Mater. Trans., JIM 30 (9) (1989) 722–725, https://doi.org/10.2320/matertrans1989.30.722.
- [41] Q. Luo, W.H. Wang, Rare earth based bulk metallic glasses, J. Non-Cryst. Solids 355 (13) (2009) 759–775, https://doi.org/10.1016/j.jnoncrysol.2009.02.006.
- [42] R.C. Sekol, G. Kumar, M. Carmo, F. Gittleson, N. Hardesty-Dyck, S. Mukherjee, J. Schroers, A.D. Taylor, Bulk metallic glass micro fuel cell, Small 9 (12) (2013) 2081–2085, https://doi.org/10.1002/smll.201201647.
- [43] G. Kumar, J. Schroers, Write and erase mechanisms for bulk metallic glass, Appl. Phys. Lett. 92 (3) (2008) 3, https://doi.org/10.1063/1.2834712.
- [44] J. Fu, Z. Li, Z. Liu, X. Li, W. Wen, F. Sun, L. Li, J. Huang, W. Ruan, S. Ren, Z. Zhang, X. Liang, J. Ma, Manufacture of porous metallic glass using dissolvable templates, Sci. China Mater. 65 (10) (2022) 2833–2841, https://doi.org/10.1007/s40843-022-2191-9.